catalysts

MDPI

Article

Boosting the H_2 Production Efficiency via Photocatalytic Organic Reforming: The Role of Additional Hole Scavenging System

Yamen AlSalka [1,2,*], Osama Al-Madanat [1,3], Amer Hakki [4] and Detlef W. Bahnemann [1,5,6,*]

1 Institut für Technische Chemie, Leibniz Universität Hannover, Callinstr. 3, 30167 Hannover, Germany; al-madanat@iftc.uni-hannover.de
2 Institute für Nanophotonik Göttingen e.V., Hans-Adolf-Krebs-Weg 1, 37077 Göttingen, Germany
3 Chemistry Department, Mutah University, Mutah, Al-Karak 61710, Jordan
4 Centre for Industrial Process Technology, Department of Chemical Engineering, KU Leuven, Agoralaan Building B, 3590 Diepenbeek, Belgium; amer.hakki@kuleuven.be
5 Laboratorium für Nano- und Quantenengineering, Leibniz Universität Hannover, Schneiderberg 39, 30167 Hannover, Germany
6 Laboratory "Photoactive Nanocomposite Materials", Saint Petersburg State University, Ulyanovskaya Str. 1, Peterhof, 198504 Saint Petersburg, Russia
* Correspondence: alsalka@iftc.uni-hannover.de (Y.A.); bahnemann@iftc.uni-hannover.de (D.W.B.)

Abstract: The simultaneous photocatalytic H_2 evolution with environmental remediation over semiconducting metal oxides is a fascinating process for sustainable fuel production. However, most of the previously reported photocatalytic reforming showed nonstoichiometric amounts of the evolved H_2 when organic substrates were used. To explain the reasons for this phenomenon, a careful analysis of the products and intermediates in gas and aqueous phases upon the photocatalytic hydrogen evolution from oxalic acid using Pt/TiO_2 was performed. A quadrupole mass spectrometer (QMS) was used for the continuous flow monitoring of the evolved gases, while high performance ion chromatography (HPIC), isotopic labeling, and electron paramagnetic resonance (EPR) were employed to understand the reactions in the solution. The entire consumption of oxalic acid led to a ~30% lower H_2 amount than theoretically expected. Due to the contribution of the photo-Kolbe reaction mechanism, a tiny amount of formic acid was produced then disappeared shortly after the complete consumption of oxalic acid. Nevertheless, a much lower concentration of formic acid was generated compared to the nonstoichiometric difference between the formed H_2 and the consumed oxalic acid. Isotopic labeling measurements showed that the evolved H_2, HD, and/or D_2 matched those of the solvent; however, using D_2O decreased the reaction rate. Interestingly, the presence of KI as an additional hole scavenger with oxalic acid had a considerable impact on the reaction mechanism, and thus the hydrogen yield, as indicated by the QMS and the EPR measurements. The added KI promoted H_2 evolution to reach the theoretically predictable amount and inhibited the formation of intermediates without affecting the oxalic acid degradation rate. The proposed mechanism, by which KI boosts the photocatalytic performance, is of great importance in enhancing the overall energy efficiency for hydrogen production via photocatalytic organic reforming.

Keywords: photocatalytic reforming; dual function photocatalysis; oxalic acid; H_2 production; energy efficiency; TiO_2

Citation: AlSalka, Y.; Al-Madanat, O.; Hakki, A.; Bahnemann, D.W. Boosting the H_2 Production Efficiency via Photocatalytic Organic Reforming: The Role of Additional Hole Scavenging System. *Catalysts* **2021**, *11*, 1423. https://doi.org/10.3390/catal11121423

Academic Editor: Stanisław Wacławek

Received: 19 October 2021
Accepted: 19 November 2021
Published: 23 November 2021

Publisher's Note: MDPI stays neutral with regard to jurisdictional claims in published maps and institutional affiliations.

1. Introduction

The solar chemical transformation processes induced by the excitation of suspended semiconductor nanoparticles have been widely studied in environmental remediation and sustainable fuel production. The interfacial charge transfer is the core of such photoinduced applications with the ability to benefit from the reduction and oxidation potentials of the photogenerated electrons and holes, respectively [1]. Among all recent existing fuels,

molecular hydrogen (H_2), a potential sustainable energy carrier, has the highest heating value of 142 MJ kg^{-1} [2]. Moreover, it yields only pure water after burning, avoiding the risk of any environmental pollution. However, in order to consider H_2 as a green fuel, it should be produced in a fully sustainable system relying on a renewable energy source such as sunlight. In this respect, the photocatalytic evolution of H_2 is a fascinating strategy aiming to convert the energy of light to chemical energy by reducing protons via a photoinduced pathway [3–5]. In most photocatalytically based H_2 evolution reactions, boosting the oxidation half-reaction by using a hole scavenger, i.e., photocatalytic reforming, and employing a specific catalyst for the reduction of protons are essential requirements to achieve acceptable efficiencies [4,6–8]. From a sustainable point of view, photocatalytic reforming of biomass-derived feedstocks is considered a practical and efficient process. Oxygenated organic compounds can be photocatalytically reformed into H_2 and CO_2 while producing close to the maximum stoichiometric amount of H_2 [9].

The explicit requirements of a photocatalyst are still an argument to explore; however, the most prevalent material that meets most of the photocatalytic prerequisites is titanium dioxide (TiO_2) [5,10]. TiO_2 is a perfect candidate for photocatalysis, owing to its price, low toxicity, stability, and well-positioned band edges that have thermodynamically adequate potentials for initiating many photocatalytic reactions [3,11,12]. However, pristine TiO_2 suffers from the rapid recombination of the photogenerated holes and electrons, besides the low reaction kinetics of proton reduction, which prompted the need to modify TiO_2 [6]. One of the effective modifying methods is surface modification by a cocatalyst, creating heterojunctions to enhance the charge separation [13,14]. Platinum nanoparticles have proven the best co-catalyst on TiO_2, promoting the H_2 evolution reaction (HER). They also hinder h^+/e^- recombination and reinforce the interfacial charge transfer to the adsorbed molecules [3,6,15].

Oxalic acid is classified as a water contaminant in the effluent of textile and metallurgy industries [16], and it is as an intermediate frequently generated upon the mineralization of organic compounds [17]. Nevertheless, oxalic acid has not been often studied as a sacrificial reagent in the photocatalytic reforming processes despite its high adsorbing affinity on TiO_2 and its foreseeable straightforward conversion. This was mainly assigned to the lack of C–H that bonded to the OOH group, which was assumed to be a prerequisite for H-abstraction [18]. However, oxalic acid has shown a higher H_2 evolution rate using irradiated TiO_2 compared to formic acid and formaldehyde [16]. Nevertheless, non-stoichiometric H_2 amounts have been reported from the photocatalytic reforming of oxalic acid [16,19], neglecting the total yields due to the long consuming periods of the organic substrate. Li et al. [16] reported no activity of H_2 production from oxalic acid over bare Degussa P25 TiO_2. However, they showed that the maximum rate of simultaneous H_2 production and decomposition of oxalic acid on Pt/TiO_2 was achieved at pH 2.9. Nevertheless, the formation of all byproducts was not well investigated. We have previously shown that the lack of an appropriate co-catalyst on TiO_2 decreases the aptitude for proton reduction because of the overpotential needed for the HER reaction. The presence of Pt NPs as co-catalysts induces the reduction of protons to produce molecular hydrogen upon the irradiation of a suspension containing oxalic acid and Pt/TiO_2 [20]. In our recent report [15], we investigated the modification of a self-prepared anatase TiO_2 and concluded that platinum nanoparticles have a superior activity compared to gold nanoparticles. We also studied the total yields of the photocatalytic reforming of oxalic acid on Pt/TiO_2, in which lower amounts of H_2 than predicted were generated. This would reflect a lower energy efficiency due to the lower produced H_2 compared to the incident photons on the photocatalytic system.

Herein, we report the photocatalytic reforming of oxalic acid using a Pt/TiO_2 photocatalyst, following the total yield of gas production and the complete decomposition of oxalic acid. Moreover, we delve into the possible mechanism and potential byproducts, by determining the photogenerated intermediates via the EPR spin-trap technique and performing isotopic substitution experiments, answering the open questions in this field.

Finally, we demonstrate one method to boost the reaction by the presence of KI, explaining the possible mechanisms. This will help to maximize the sustainable production of H_2 from organic wastes and provide a more energy-efficient system.

2. Results and Discussion

2.1. The Fate of Oxalic Acid during the Photocatalytic Reforming

In order to pursue the photocatalytic reforming of oxalic acid, the products present in the gas phase and liquid phase were detected using the QMS and the HPIC, respectively. Figure 1 displays the time course of the consumption of oxalic acid over illuminated Pt/TiO_2 together with the development of the photocatalytically generated products relative to the initial oxalic acid amount. The curves for H_2 and CO_2 in Figure 1 result from the integration of the production rates. Both H_2 and CO_2 gases evolved immediately upon turning on the irradiation without any induction period. The time course of gases evolution shows a maximum production after 400 min, at which no oxalic acid was detected in the aqueous phase. However, tiny amounts of CO_2 evolved after 400 min, even though no more oxalic acid had been detected in the solution. This can be partially due to the intermediates, but mainly due to the amount of oxalic acid adsorbed on TiO_2 because of the very low concentration of formed formic acid as a byproduct. After 500 min, a deterioration in the rates in the evolution of gases was observed until reaching non-detectable levels. It is worth to mention that the experiment was continued until 720 min, and no changes were noticed. Simultaneously, the amount of oxalic acid in the solution gradually decreased throughout the illumination as revealed from the HPIC measurements. Figure 1 indicates that complete consumption of oxalic acid was achieved in less than 500 min of irradiation. Figure 1 additionally demonstrates a correlation between the behavior of gas production and the attitude of oxalic acid degradation, in which after 400 min, a sharp decline in the gas evolution is associated with the almost complete degradation of oxalic acid. HPIC was also used as a detection method for the byproducts in the solution, in which formate was confirmed as the main byproduct. The time-profile of formate release is shown in Figure 1. Formate was continuously produced to reach the maximum amount after 300 min, then a decrease in its detected amount was observed. However, around a 100 times lower amount of formate was produced in comparison to the converted oxalic acid and to the evolved H_2 and CO_2. It is worth to mention that even though the experiments were done in the absence of O_2, a total decomposition of organics was achieved over the employed Pt/TiO_2.

2.2. Stoichiometric and Mechanistic Investigations

The amounts of H_2 and CO_2 produced upon the complete conversion were found to be 40.1 ± 1.4 and 110.0 ± 3.2 µmol, respectively. It is obvious that the amount of CO_2 evolved corresponds to the theoretical amount, which is expected to result from the complete degradation of oxalic acid, as per Equation (1). Remarkably, the amount of H_2 evolved was lower than the theoretically calculated amount. The experimentally obtained H_2:$OA_{(total)}$ ratio was 0.72, which is lower than 1, as theoretically would be expected. However, the CO_2:OA(total) ratio was 1.98, which is very close to the theoretical ratio of 2. This indicates that under our experimental conditions, the surface oxidation of oxalic acid is more effective than the reduction of protons on Pt NPs, and the complete consumption of oxalic acid shows about 30% lower H_2 production than foreseeable. Thus, a total decomposition of oxalic acid was achieved over the employed Pt/TiO_2. We reported such lower stoichiometric H_2:OA ratios (30 to 40%) using Pt/TiO_2 in our previous works [15,20]. Several studies have also reported non-stoichiometric data upon the photocatalytic reforming of oxalic acid. The long-term illumination of a suspension containing Pt-TiO_2 and 0.05 mol L^{-1} oxalic acid resulted in a ratio of 0.64 [21], while the illumination of a suspension containing 3 mmol L^{-1} oxalate, a photocatalyst composed of Pt NPs and 2-phenyl-4-(1-naphthyl)quinolinium ion ($QuPh^+$-NA), led to 80% of the stoichiometric amount [19].

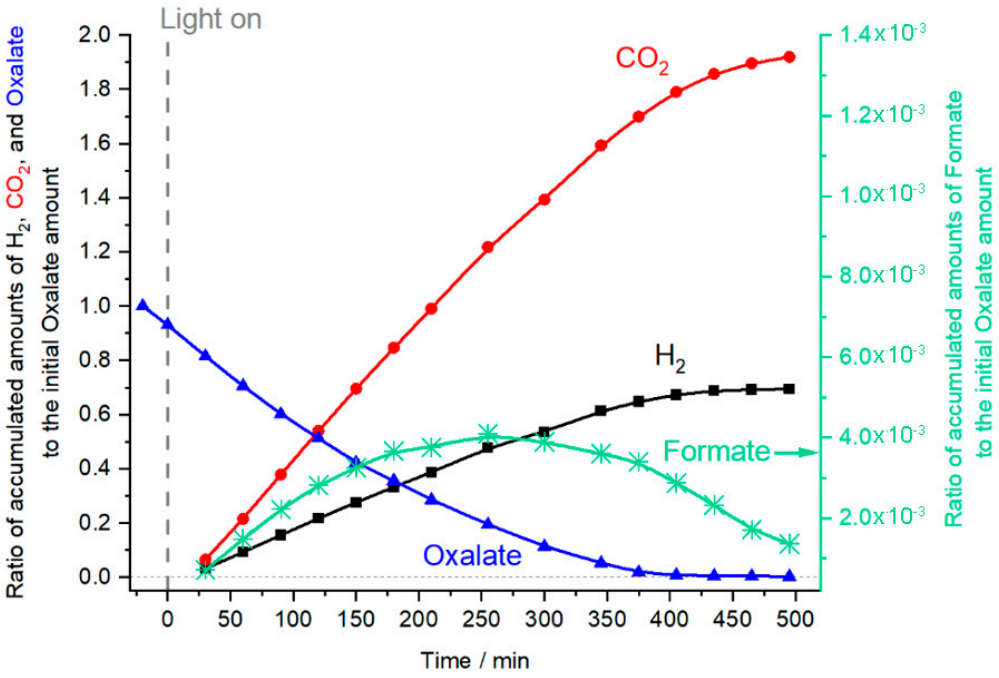

Figure 1. Relative amounts of evolved H_2, CO_2, and formate, besides decomposed oxalate, to the initial amount of oxalic acid. A 50 mL aqueous suspension containing 1.11 mmol L^{-1} oxalic acid and Pt/TiO_2 at pH ~3. A longpass filter with a cut-on wavelength of 310 nm was used.

Although the hydrogen production was lower than expected, the photoreforming of oxalic acid can be effectively performed. However, recovering this lost amount of produced H_2 would enhance the total energy efficiency of the system in term of photons to H_2 production. Therefore, it is very important to investigate the reason of such a deviation in the efficiency in order to boost it up. For this purpose, isotopic and EPR experiments were employed.

$$H_2C_2O_4 \rightarrow H_2 + 2CO_2 \quad (1)$$

2.3. Isotopic Studies

Isotopic substitution studies were conducted in several suspensions containing D_2O-H_2O mixtures at different ratios to pursue the source of the evolved H_2 and, thus, to understand the contribution in this deviation from the stoichiometric ratio. Figure 2 shows the detected CO_2 (a), HD (b), H_2 (c), and D_2 (d) gases upon illumination of oxalic acid dissolved in different D_2O-H_2O mixtures. Besides H_2 and CO_2, both HD and D_2 gases were detected by the QMS whenever D_2O was present as a co-solvent. As presented in Figure 2, when the D_2O fraction increased, a progressive decrease in the rate of the gas evolution and in the total amount of evolved H_2 and CO_2 was observed. Considering the use of H_2O and D_2O as pure solvents, the ratio between the amounts of evolved CO_2 after 250 min was ~1.5. Remarkably, neither H_2 nor HD evolved in pure D_2O solvent. These results suggest that the water should be the source of the H_2 evolution from oxalic acid, similar to the case of reforming of methanol [22]. However, H_2 production was stopped upon the complete consumption of oxalic acid. Moreover, O_2 was not simultaneously evolved, even when a tiny amount of oxalic acid existed in the solution, denying again any photocatalytic water splitting. Therefore, the contribution of water in this system is due to a proton exchange reaction. The solvent's isotopic species are dominant, and the rates of proton-exchange reactions are quite high. Consequently, the proton-exchange reaction can mask the actual source of the hydrogen, which could originate from oxalic acid molecules. It has been well established that D_2O adsorption on TiO_2 in the dark leads to an isotopic exchange of the OH group (Ti-OH + OD^- → Ti-OD + OH^-) [23]. Therefore, the photogenerated holes can be trapped on the surface OD group as $^{\bullet}$OD radicals. Because

such isotopic exchanges are surface reactions, the kinetic isotopic effect is also anticipated during the photocatalytic experiment. Considering what has been discussed above, the actual origin for H_2 is most likely oxalic acid. When different mixtures of H_2O and D_2O were used as solvents, various mixtures of H_2, HD, and D_2 gases were observed that met the isotopic fraction in the solvent. Only H_2 and HD, but not D_2, were detected when the D_2O percentage was less than 50% in the H_2O-D_2O composition mixtures, which could be due to the preferential protium reduction [24].

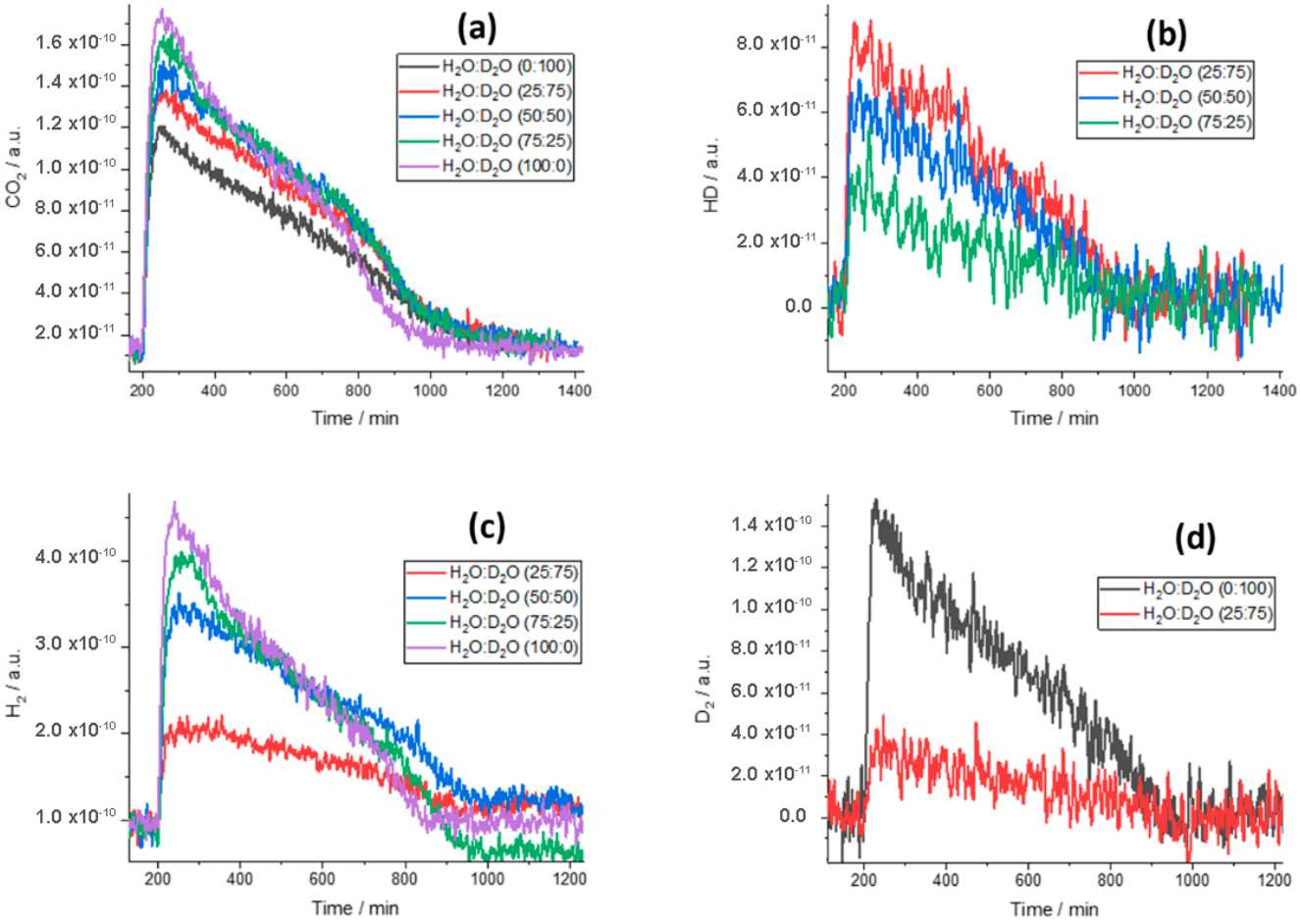

Figure 2. Quadrupole mass spectroscopy (QMS) signals for the evolved CO_2 (**a**), HD (**b**), H_2 (**c**), and D_2 (**d**) formation in different H_2O/D_2O mixtures over Pt/TiO_2 during the photocatalytic reforming of oxalic acid. The intensities of the produced gases have arbitrary units since each gas has a special concrete response value.

The decrease in the rate of CO_2 and H_2 evolution due to the use of D_2O, as shown in Figure 2a,c, ought not to be interpreted as hindrance of $^{\bullet}$OH radicals generation. This is the issue when formaldehyde [23], methanol, and benzene [25] were used in the presence of Pt/TiO_2, where the retardation of $^{\bullet}$OH slows the rate of the reaction. Herein, $^{\bullet}$OH radicals have a secondary role in oxalic acid decomposition because the surface charge transfer of adsorbed oxalic acid with the photogenerated holes is the dominate mechanism. Hence, the observed kinetic isotope effect is related, most likely, to the proton reduction, which is the rate-determining step [24,26]. However, more investigations are required to establish this conclusion.

2.4. The Role of Intermediates

As it turned out, the cause of the lower amounts of H_2 cannot be directly traced back to the formation of byproducts, but there is undoubtedly another reason related to the formation of H_2, as the stoichiometric amount of CO_2 has been proven experimentally and

the formate completely decomposed. Thus, the mechanism of the formation of molecular hydrogen and other byproducts was investigated employing EPR spectroscopy. The nature of the photogenerated species was specified using DMPO as a spin-trapping agent. EPR measurements were performed in the absence of O_2 before and during the UV irradiation of an aqueous suspension of 1 g L^{-1} Pt/TiO_2 and 5.5 mmol L^{-1} oxalic acid at pH 3. No EPR signal was detected in the dark, while after 1 min of irradiation a complex signal was recorded and increased during the irradiation, as shown in Figure 3a. This complex signal refers to more than one spin adduct being simultaneously produced and overlapping with each other. As a consequence of $^{\bullet}CO_2^-$ radicals generation, the appearance of the DMPO$^{\bullet}$-CO_2^- spin adduct is expected [15]. The simulation of the EPR spectrum in Figure 3a shows a mixture of three adducts, and each has a six-line signal; DMPO$^{\bullet}$-CO_2^-, DMPO$^{\bullet}$-CHO, and DMPO$^{\bullet}$-(CO-CO_2^-) having hyperfine parameters of (a^N = 15.53 G, $a_\beta{}^H$ = 18.47 G), (a^N = 15.6 G, $a_\beta{}^H$ = 21.10 G), and (a^N = 15.7 G, $a_\beta{}^H$ = 23.25 G), respectively [27], as shown in Figure 3b. Therefore, in addition to $^{\bullet}CO_2^-$ radicals, other carbon-centered radicals were simultaneously produced upon the irradiation of the suspension. Our results correlate with the theoretical calculations of a possible direct oxidation and reduction of oxalic acid on the surface of titanium dioxide by the photogenerated species [28]. The formation of other byproducts such as hydroxyalkyl radicals detected by the EPR experiment can be explained by the cleavage of the bonding between the OH group and the rest of adsorbed oxalic acid due to the irradiation. The formed surface radicals can react with hydrogen atoms to form adsorbed glyoxylate species, as shown in Scheme 1. Hence, the generation of such hydroxyalkyl radicals, which can be converted to formic acid, consumes the hydrogen atoms. This mechanistic pathway has also been predicted by the combination of Attenuated Total Reflectance-Fourier-transform infrared (ATR-FTIR) studies and the theoretical MSINDO-CCM calculations [28].

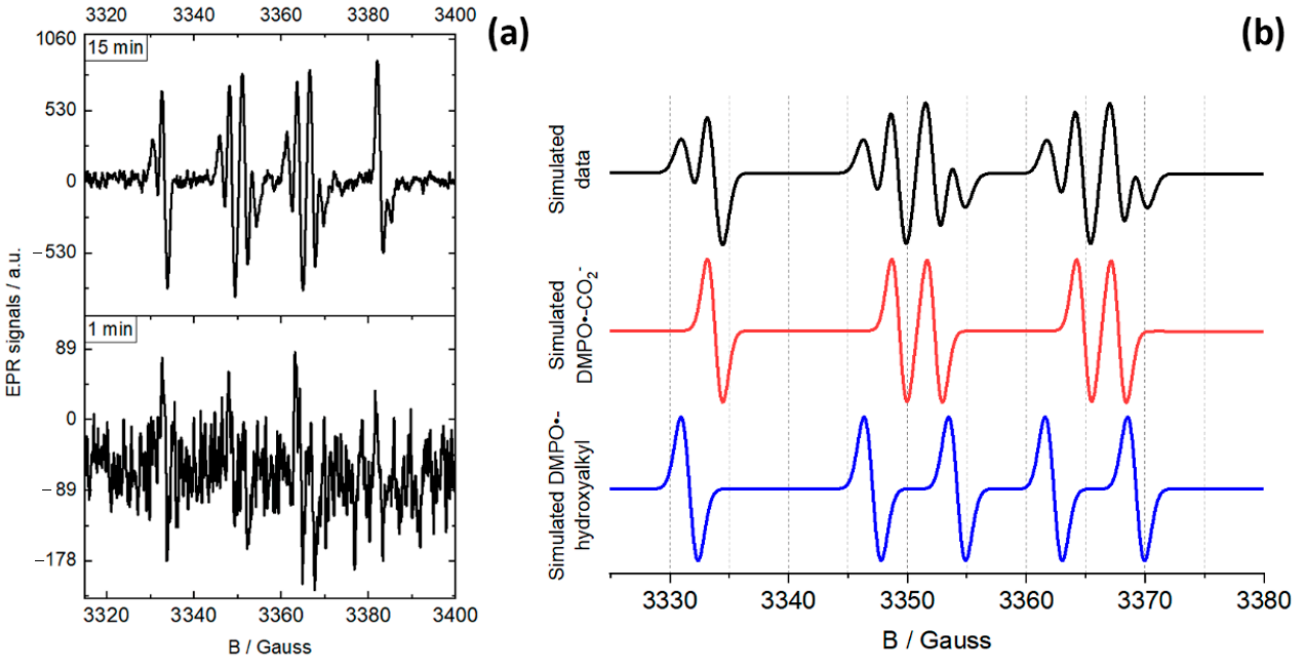

Figure 3. EPR spin trap spectra in N_2 atmosphere during UV irradiation; (**a**) experimental spectra; and (**b**) simulated spectra. The suspension consisted of oxalic acid (5.5 mmol L^{-1}), DMPO (0.8 mmol L^{-1}), and Pt/TiO_2 (1 g L^{-1}). The extracted spectra in Figure 3b were normalized to demonstrate the overlap between the diverse species.

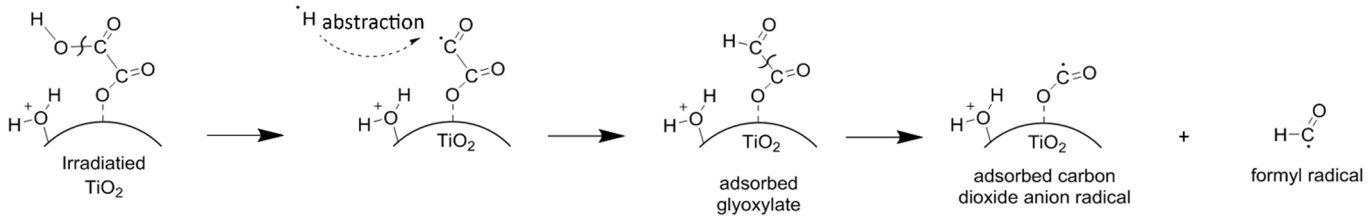

Scheme 1. The mechanism proposed for the cleavage of C–O bonds before the addition of hydrogen atoms to produce adsorbed aldehyde molecules. Adapted from [15,28], copyright 2020, American Chemical Society.

Based on the discussed results and on the EPR investigations, the degradation of oxalic acid on the surface of TiO_2 can be accomplished through different pathways. Here, hydrogen oxalate $HC_2O_4^-$ is dominant in the suspension at pH 3 ($pK_{a1(OA)}$ = 1.25) [29]. These species adsorb on the surface of TiO_2 and react directly with the photogenerated holes [28] to produce hydrogen oxalate radicals $HC_2O_4^{\bullet}$ (Equation (2)). These radicals can also be produced through an indirect hole transfer oxidation by the hydroxyl radicals generated on the titanium dioxide surface (Equation (3)) [30,31]. Through a photo-kolbé reaction mechanism, hydrogen oxalate radicals are further degraded to form CO_2 and carbon dioxide anion radicals $^{\bullet}CO_2^-$ via the formyloxyl radical $HCO_2^{\bullet}$ (Equation (4)). $^{\bullet}CO_2^-$ are highly reductive radicals ($E^0 = -2.0$ V) [32], and they have been shown to induce the current doubling effect (Equation (5)) through the injection of their electrons in the conduction band of TiO_2 [33]. $^{\bullet}CO_2^-$ radicals can also initiate the formation of formate, either by their reaction with $H^{\bullet}$ radicals (Equation (6)) or via H-subtracting of water (Equation (7)). Previous reports have also showed that the degradation of elementary di-carboxylic acids in the absence of O_2, e.g., oxalic acid, led to the generation of their corresponding monocarboxylic acids [34]. For example, formic acid and formaldehyde were detected by ^{1}H NMR during the irradiation of oxalate solution containing $QuPh^+$–NA and platinum nanoparticles. The results had been explained by considering the oxalate as a one-electron donor, an assuming that the reduction of $^{\bullet}CO_2^-$ radicals takes place through hydrogen adsorbed on the surface of platinum [19]. The disproportionation of $^{\bullet}CO_2^-$ radicals (Equation (8)) induces also the generation of CO_2 and formate, competing with the current doubling phenomenon [15]. An adsorbed aldehyde molecule can be produced, as has been predicted via cleavage of the C–O bond by the addition of hydrogen atoms, as shown in Scheme 1 [28].

The proposed equations and mechanisms are based on the ATR FT-IR studies of oxalic acid on TiO_2 under UV light together with quantum chemical calculations done by Mendive et al. [28]. Oxalic acid was found to adsorb as bidentate and monodentate structures, with the latter as the preferable complex on anatase TiO_2. In their studies, the photogenerated holes were shown to be trapped on O–O or on C–C bonds. On the other hand, they found that Ti–Ti, C–C, or C–O bonds had been found to be the possible trapping sites of the photogenerated electrons. Thus, h^+/e^- pairs initiate a direct oxidation/reduction of adsorbed oxalic acid, while a secondary role of the attack of OH radicals has been proved.

Owing to the discussed data, the possible reasons for the non-stoichiometric yield of hydrogen gas are the competitive consumption of electrons or $H^{\bullet}$ radicals by additional reactions and the disproportionate amount of $^{\bullet}CO_2^-$ radicals reducing the contribution of the current doubling. The reaction mechanisms in the presence of $^{\bullet}CO_2^-$ radicals can be, indeed, complicated. On the one hand, an injection of $^{\bullet}CO_2^-$ radical electrons in the CB of TiO_2 leads to the current doubling, in which one injected electron generates H_2 with the contribution of another photogenerated electron from TiO_2, leading to H_2:OA = 1. On the other hand, in the absence of the current doubling from $^{\bullet}CO_2^-$ radicals, two photogenerated electrons are essential for generating one H_2 molecule, and thus the H_2:OA = 0.5. In our case, we assume that both mechanisms simultaneously happened to different extents related to the concentration of oxalic acid in solution. Thus, the lower

H_2 can be explained by the imperfection of the current doubling contribution. Such a deficiency of the current doubling has been previously reported in the case of methanol and has shown to be related to the pH of the solution, the amount of methanol, and the photon flux [35]. Moreover, in another study, the photo-oxidation of different organic substrates using TiO_2 electrodes has never shown a maximum current doubling, rather an excess of ~50% in the photocurrent has been recorded [36]. Other reasons for the deficiency of H_2 are the adsorption of hydrogen on the surface of Pt NPs, retarding the evolution of molecular hydrogen, and/or the solubility of H_2 gas in the aqueous solution. Owing to the fact that argon was purged in the gas phase over the solution, the amount of dissolved gas, i.e., H_2, is proportional to its partial pressure in the gas phase. Applying Henry's law $C = P/K_H$, where K_H = 1282.05 L atm mol^{-1} [37], the dissolved H_2 at the maximum evolution rate is estimated to be 0.02 µmol, which corresponds to 6.25% from the H_2 amount at maximum evolution. However, the continuous stirring of suspension can disturb the stability of dissolved bubbles in aqueous media, making the dissolved H_2 amount lower than the estimated amount.

The presence of different oxidation states of platinum on TiO_2 can also contribute to the lower H_2 amounts. It is well known that platinization of TiO_2 by the photodeposition method through the photo-reduction of chloroplatinic acid solution results in different Pt oxidation states, i.e., Pt^0, PtO, and PtO_2. The reduction of such platinum oxides can, in turn, consume a part of the photogenerated electrons, leading to a decrease in electrons available for the reduction of protons. The reduction of surface platinum oxide by TiO_2 photogenerated electrons has been recently reported by Puga et al. [38], who noticed that the in situ surface reduction of platinum oxide species on TiO_2 contributed to a little H_2 formation in the presence of Rhodamine B solution. However, we think that such a phenomenon has limited effects, in our case, especially because we have reported earlier, using the X-ray photoelectron spectroscopy (XPS) technique, a predominant distribution of Pt^0 on the surface of the self-prepared anatase TiO_2 [15]. In addition, if PtO_2 is considered as the lone platinum type on the surface, it will consume 1.1 µmol of electrons as the maximum amount needed to reduce it in our experimental conditions. Hence, the reduction of surface PtO_2, if present, can decrease the H_2 by a maximum amount of 0.55 µmol, which is within our experimental error.

In another experiment, a higher concentration of oxalic acid was used, i.e., 100 mmol L^{-1}, and the illumination lasted for 1200 min. Although such a period was not enough to consume all oxalic acid, stable rates of H_2 and CO_2 were achieved, confirming a steady production. Moreover, higher amounts of both gases were acquired because most photocatalytic paths are of the Langmuir type. Interestingly, the CO_2:H_2 ratio was about 2 after 20 h of photoreforming of the concentrated solution, which is closer to the stoichiometric calculation. We think that a higher and steady formation of CO_2 radical anions occurred in such a higher concentration of oxalic acid, increasing the current doubling-like effect and, hence, the electrons available for the reduction of protons. A similar behavior has been reported in the literature through 1.6 times enhancement in the photogenerated current of TiO_2 electrode due to a 5-times increase in the concentration of different organic substrates [36].

$$HC_2O_4^- + TiO_2(h^+) \rightarrow HC_2O_4^\bullet + TiO_2 \quad (2)$$

$$HC_2O_4^- + {}^\bullet OH \rightarrow HC_2O_4^\bullet + OH^- \quad (3)$$

$$HC_2O_4^\bullet \rightarrow CO_2 + HCO_2^\bullet \rightleftharpoons {}^\bullet CO_2^- + H^+ \quad (4)$$

$${}^\bullet CO_2^- + TiO_2 \rightarrow CO_2 + TiO_2(e^-) \quad (5)$$

$${}^\bullet CO_2^- + H^\bullet \rightarrow HCO_2^- \quad (6)$$

$${}^\bullet CO_2^- + H_2O \rightarrow HCO_2^- + {}^\bullet OH \quad (7)$$

$$2{}^\bullet CO_2^- + H^+ \rightarrow CO_2 + HCO_2^- \quad (8)$$

2.5. Maximizing the Total Yields by the Addition of KI

As revealed from the previous discussion, the continuous feeding of the hole scavenger, rather than the effects of the surface or the co-catalyst, has, most likely, the essential role in maintaining a constant rate of photocatalytic production of gases, which yields closer values to the theoretical calculations. We have noticed that the H_2 evolution was dramatically decreased when the amount of oxalic acid became low. Thus, another reason of lower H_2 quantity can be traced back to the kinetics of proton reduction, which might be lower than the kinetics of hole scavenging in the low oxalic acid regime as a reason of its photocatalytic degradation. When the amount of oxalic acid is relatively small, either the photo-generated electrons accumulate on the surface of Pt-NPs and are not directly consumed by the reduction reaction, or the kinetics of the transfer of photo-generated electrons to Pt-NPs becomes lower due to the faster recombination of the photo-generated charge carriers, i.e., the recombination is dominant. As a hole scavenging assistant, KI was additionally used in the oxalic acid system; thus, the photocatalytic experiments were repeated in the presence of 20 mmol L^{-1} KI. Different kinetics of gas generation are noticed in Figure 4a due to the presence of two electron donors in the system. While the kinetics of CO_2 evolution changed just after 400 min of irradiation, higher kinetics of H_2 evolution was clearly noticed after 50 min of irradiation. During the first 50 min, negligible changes in the amounts evolved were observed between both cases, as can be seen in Figure 4b, in which almost identical amounts of gases evolved using Pt/TiO_2. Interestingly, after 50 min of irradiation, higher amounts of gases, especially H_2, were generated compared to the previous experiment until no-detection of gases was possible after 500 min. KI acts seemingly as an effective hole scavenger when the amount of oxalic acid becomes less as the illumination continues, maintaining the effective separation between the charge carriers during the entire period of irradiation until the complete degradation of oxalic acid, hence, generating the H_2 with the most possible efficiently. The total amounts of H_2 and CO_2 produced while using KI in addition to oxalic acid reached 55.14 ± 1.410 and 112.1 ± 3.141 µmol, respectively. Here, CO_2:H_2, and H_2:$OA_{(total)}$ reached the theoretical ratios, i.e., 2.033 and 0.993, respectively. These values confirm a complete photocatalytic reforming of oxalic acid, reaching the stoichiometric H_2 amount.

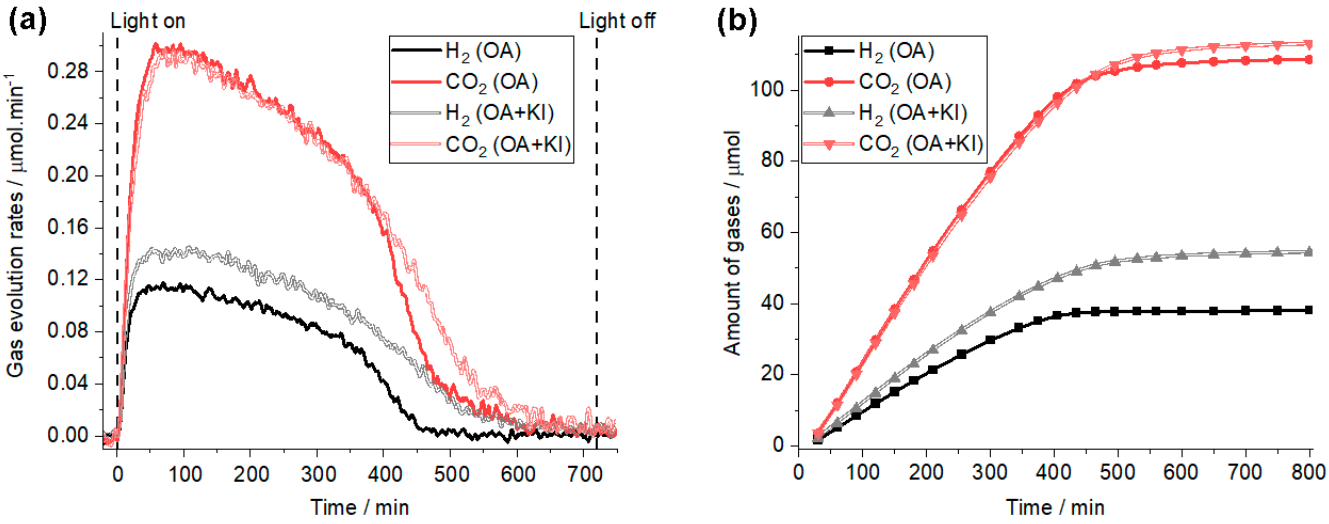

Figure 4. QMS signals (**a**) for the evolution of H_2 and CO_2 from the reforming of oxalic acid with and without the presence of 20 mmol L^{-1} KI. The evolved amounts (**b**) of H_2 and CO_2. A 50 mL aqueous suspension containing 1.11 mmol L^{-1} oxalic acid at pH ~3 on Pt/TiO_2. A longpass filter with a cut-on wavelength of 310 nm was used.

Regarding the CO_2:H_2 ratio, two plots are presented in Figure 5 describing the changes in this ratio during the irradiation time in both cases. Remarkably, in the absence of KI, the ratio was always higher than 2. During the first 50 min, the ratio was close to the theoretically predicted value, followed by a notable increase, especially after 400 min

of irradiation. This behavior confirms, as we discussed earlier, the evolution of a lower H_2 amount than expected from the photocatalytic reforming of oxalic acid, particularly when the concentration of oxalic acid was lower. However, during the first 120 min of irradiation in the presence of KI, the ratio of CO_2:H_2 was lower than 2, indicating a higher H_2 production than expected, to reach a steady-state of ratios close to 2 until the total consumption of oxalic acid in suspension. We believe that KI does not compete with oxalic acid for the photogenerated holes; however, it offers better separation between the photogenerated charge carriers in the low oxalic acid regime and prolongs the life of electrons to be optimally collected by Pt NPs. Hence, the presence of KI would maintain the continuous availability of electrons regardless of the amount of oxalic acid in the suspension. Despite that KI serves as a good hole scavenger, its presence did not interfere with the photocatalytic degradation of oxalic acid, as shown from the experimental results. This could be related to the presence of preferable adsorption sites of oxalic acid, although other sites are still available for the adsorption of KI to be oxidized. Thus, in the competition adsorption condition of KI and oxalic acid, the latter seems to preferably be adsorbed on specific surface sites to work, hence, as a hole scavenger regardless of the existence of KI.

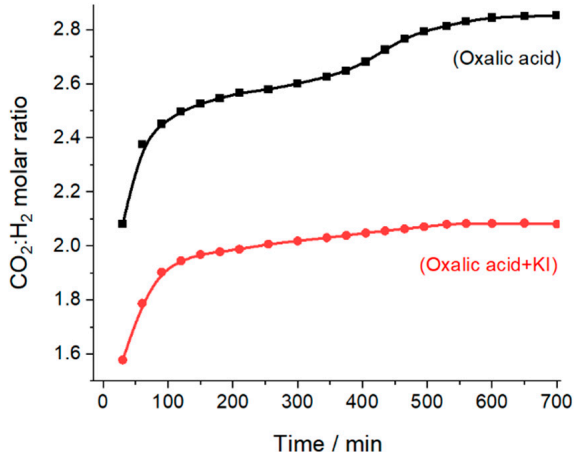

Figure 5. The ratio between the evolved CO_2/H_2 amount with and without the presence of KI. A 50 mL aqueous suspension containing 1.11 mmol L^{-1} oxalic acid at pH ~3 on Pt/TiO_2. A longpass filter with a cut-on wavelength of 310 nm was used.

Furthermore, KI can disturb the hydrogen adsorption on Pt NPs, affecting the H–Pt bonding and reducing the ability of hydrogen adsorption. It was well established that chemisorbed iodide ions diminish the amount of adsorbed hydrogen on the surface of platinum [39]. A repulsive interaction between the halogen atoms and the adsorbed hydrogen on the surface of Pt has also been reported. Therefore, H-I co-adsorption on Pt has been found to have a competitive characteristic [40]. Hence, KI hinders the adsorption of hydrogen on Pt NPs, which positively affects the energy efficiency. Noteworthy, no O_2 was photocatalytically evolved in the presence of KI, even in the low oxalic acid regime. Moreover, no hydrogen gas was detected when using KI alone as an electron donor or after the total consumption of oxalic acid in the presence of KI. These observations confirm the indispensable function of oxalic acid in producing H_2 and prove that the photocatalytic water splitting in the presence of both hole scavengers looks unreasonable.

The tracking of the oxalic acid amount by HPIC was unfortunately impossible because of the interference caused by the broad peak of KI. However, no formate peaks were detected by the HPIC during the irradiation, which indicates that the production of formate as a byproduct is minimal when KI is present in the suspension. This could be due to the rapid conversion of $^{\bullet}CO_2^-$ radicals to CO_2 rather than their reactions with $^{\bullet}H$ atoms. EPR spin-trap measurements were performed as described before but in the presence of KI in the suspension. While no EPR signal was detected in the dark, the signal first appeared after 4 min of irradiation, as shown in Figure 6, and increased over time. Two remarkable

differences are clearly seen when comparing the EPR spectra without and with the use of KI, respectively. While two overlapped adducts were produced in the first case (see Figure 3), the DMPO$^{\bullet}$-CO_2^{-} spin adduct was the only signal detected in the presence of KI. However, the intensities of EPR spectra are significantly lower. This indicates a different pathway, and lower $^{\bullet}CO_2^{-}$ radical production rates have been observed when KI was added to the suspension. The outcomes from HPIC and EPR measurements prove that the use of KI inhibits the release of the byproducts since only $^{\bullet}CO_2^{-}$ radicals were detected during the illumination. This can be explained by the conversion of the extremely reductive $^{\bullet}CO_2^{-}$ radicals to CO_2 due to their rapid reaction with I_2, which is a product of KI oxidation. This mechanism is presented in Equations (9)–(14), respectively [5,41–44].

$$2\,I^- + h^+_{VB} \rightarrow I_2^{-\bullet}\ (K = 3.2 \times 10^9) \quad (9)$$

$$2\,I_2^{-\bullet} \rightarrow I_3^- + I^- \quad (10)$$

$$I_3^- \rightleftharpoons I^- + I_2 \quad (11)$$

$$I_3^- + e^- \rightarrow I_2^{-\bullet} + I^- \quad (12)$$

$$I_2 + e^- \rightarrow I_2^{-\bullet} \quad (13)$$

$$^{\bullet}CO_2^- + I_2 \rightarrow I_2^{-\bullet} + CO_2\ (K = 7 \times 10^9) \quad (14)$$

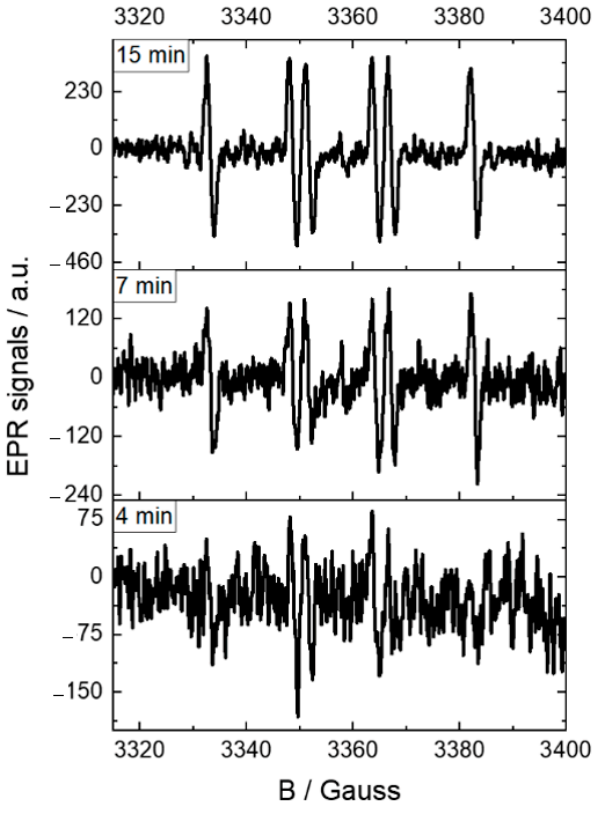

Figure 6. EPR spin trap experiments in N_2 atmosphere for a UV-irradiated suspension containing oxalic acid (5.5 mmol L^{-1}), 20 mmol L^{-1} KI, DMPO (0.8 mmol L^{-1}), and Pt/TiO_2 (1 g L^{-1}).

3. Experimental Section

3.1. Materials

The used chemicals were employed as purchased without purification. Deionized water (18.2 MΩ·cm at 25 °C) was generated using a Milli-Q device (Merck Millipore, Germany). Oxalic acid (≥99%), chloroplatinic acid hydrate $H_2PtCl_6{\cdot}xH_2O$ (≥99.9%), potassium iodide (≥99%), deuterium oxide (99.9 atom % D), and 5,5-dimethyl-1-pyrroline-

N-oxide (DMPO) were purchased from Sigma-Aldrich (Merck, Germany). Anhydrous sodium carbonate (≥99%) was purchased from Carl-Roth (Germany).

Anatase TiO_2 was synthesized according to our previous work, having the capability to photo-catalyze the H_2 generation in the presence of an electron donor [12,15]. Briefly, the triblock copolymer F-108 was dissolved in ethanol before adding acetylacetone and the precursor $TiCl_3$. The mixture was self-assembled at 40 °C for 24 h followed by a calcination period of 12 h at 400 °C. The material was then modified by platinum nanoparticles ($Pt_{0.25\%}/TiO_2$) using a photodeposition method [20]. Typically, the TiO_2 was added to a de-aerated 10% (*v*/*v*) aqueous methanol solution. The calculated amount of $H_2PtCl_6 \cdot xH_2O$ was then added, then the suspension was kept at 15 °C and irradiated with a Philips CLEO UV(A) lamp. The solid was, afterward, separated by centrifugation and dried at 100 °C for 24 h after several washing and centrifugating steps. The thus-obtained TiO_2 sample showed good crystallinity of the TiO_2 and homogenous spreading of Pt nanoparticles, having particle sizes of 1–5 nm, as revealed from the TEM images shown earlier [15].

3.2. Photocatalytic Experiments

A 65 mL double-jacket glass photoreactor attached to a quadrupole mass spectrometer QMS (Hiden HPR-20, Warrington, UK) was used (Figure 7) to analyze the evolved gases. A continuous flow at 5.0 cm^3 min^{-1} of argon over the reaction mixture was used as a carrier gas. Such a continuous setup permits the long-term operation without facing the overpressure problem inside the reactor [20,22]. Typically, 25 mg of $Pt_{0.25\%}/TiO_2$ was suspended in 50 mL of oxalic acid solution at pH ~3 that contains 1 mmol L^{-1} KNO_3, preserving the ionic strength [45]. The initial concentration of oxalic acid was adjusted to 1.11 $mmol^{-1}$ in most experiments unless otherwise mentioned, and the temperature of suspension was kept at 20 °C. The light source consisted of Osram XBO 1000 W Xenon Arc Lamp in a housing model Müller LAX 1000 with measurements at 310 nm to avoid the photolysis of oxalic acid [46] and nitrate, preventing any homogeneous photolysis process. The blank experiments confirmed a negligible effect of the presence of nitrate on the photogeneration of H_2. A photon flux of $I_0 = 9.83 \times 10^{-5}$ mol m^{-2} s^{-1} in the window of the photoreactor was calculated based on irradiance between 320 nm and 380 nm, which has a value of 31 mW cm^{-2}. This corresponds to 49.4×10^{-9} $mol_{(photons)}/s$ when ignoring the reflection and scattering effects.

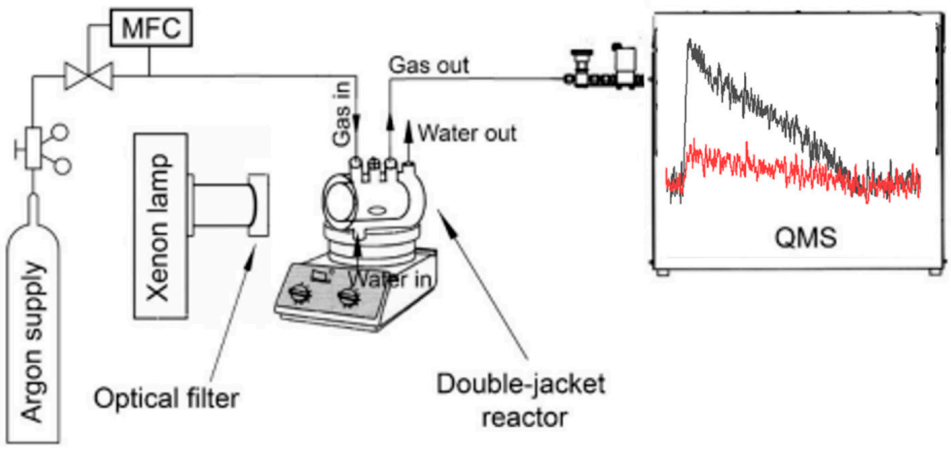

Figure 7. Experimental setup used for the continuous detection of the photocatalytic gas evolution. Adapted from [15], copyright 2020, American Chemical Society.

Before irradiating the system, a dark stabilization for at least 2 h was performed until a steady baseline was obtained, reaching the adsorption equilibrium. A stable baseline was achieved when undrift signals for each gas, having minimal noise, were maintained for 30 min. Afterward, the suspension was irradiated, and the evolved gases were quantified after calibrating the QMS with argon-diluted standard gases (Linde Gas, Pullach, Germany).

The dissolved byproducts along with the amount of oxalic acid were quantified by high-performance ion chromatography HPIC (Dionex ICS-1000, Thermo Scientific, Waltham, MA, USA) having a temperature-controlled conductivity cell (35 °C) and equipped with an electro-regenerated suppressor. A 0.5 mL volume was periodically sampled and filtered, proceeding with the injection into the HPIC. A solution of Na_2CO_3 (9 mmol L^{-1}) was used as a mobile phase, while an Ion Pac AS9-HC 2 × 250 mm column together with Ion Pac AG9-HC 2 × 50 mm as a pre-column were employed as a stationary phase. Each photocatalytic experiment was repeated twice, having an estimated error of around ±5%.

3.3. Electron Paramagnetic Resonance (EPR) Experiments

EPR surveys were accomplished employing an X-band MiniScope MS400 spectrometer (Magnettech GmbH, Bruker, Berlin, Germany) using a microwave frequency of 9.42 GHz. The irradiation was achieved through a UV spot-light using a super-quiet mercury-xenon lamp (LC8, Hamamatsu, 200 W). The nature of the photogenerated species during the irradiation was investigated using the spin-trap method and DMPO as a spin-trapping agent. Typically, sealed capillaries were employed having the suspensions in free O_2 conditions. Each suspension consisted of 1 g L^{-1} of Pt/TiO_2, 5.5 mmol L^{-1} of oxalic acid adjusted at pH ~3, and 0.8 mmol L^{-1} of DMPO. A center field of 335.4086 mT with gain of 5 were used to acquire the data employing the following parameters: sweep time of 15 s having 4096 data points, modulation amplitude of 0.2 mT, and microwave power of 10 mW. The Easy Spin simulator was utilized to fit the spectral data form the spin-trap experiments [47].

4. Conclusions

This work demonstrates the ability to produce H_2 through the photocatalytic reforming of oxalic acid on Pt/TiO_2, despite about a 30% decrease in the amount of H_2 produced compared to the amount expected. Although a tiny amount of formate was formed as a by-product, oxalic acid and formate completely decomposed during the experiment; thus, TiO_2-photocatalysis can be considered as a good technique to decompose the organic pollutants even in the absence of O_2. The presence of KI, besides oxalic acid, maximized the H_2 amount mainly by maintaining the hole scavenging strength in the system without competing with oxalic acid for the photogenerated holes. This ensures the continuous separation of charge carriers regardless of the amount of oxalic acid, hence guaranteeing the persistent availability of electrons for the reduction of protons. Moreover, KI can disturb the H–Pt bonding, decreasing the probability of the adsorption of hydrogen on Pt co-catalysts. Undoubtedly, recovering the amount of H_2 lost, by using KI as an additional hole scavenger, reflects a 30% enhancement in the overall energy efficiency of the system in terms of photons to H_2 production.

Author Contributions: Conceptualization, methodology, formal analysis, investigation, writing—original draft preparation, Y.A.; writing—review and editing, Y.A., O.A.-M. and A.H.; supervision, D.W.B. All authors have read and agreed to the published version of the manuscript.

Funding: This research received no external funding.

Data Availability Statement: Data is contained within the article.

Acknowledgments: Yamen AlSalka thanks the financing from the Deutscher Akademischer Austauschdienst (DAAD) and the German Federal Foreign Office. Osama Al-Madanat thanks the financing from the Katholischer Akademischer Ausländer-Dienst (KAAD).

Conflicts of Interest: The authors declare no conflict of interest.

References

1. Jeon, T.H.; Koo, M.S.; Kim, H.; Choi, W. Dual-Functional Photocatalytic and Photoelectrocatalytic Systems for Energy- and Resource-Recovering Water Treatment. *ACS Catal.* **2018**, *8*, 11542–11563. [CrossRef]
2. Niaz, S.; Manzoor, T.; Pandith, A.H. Hydrogen storage: Materials, methods and perspectives. *Renew. Sustain. Energy Rev.* **2015**, *50*, 457–469. [CrossRef]
3. Hakki, A.; AlSalka, Y.; Mendive, C.B.; Ubogui, J.; dos Santos Claro, P.C.; Bahnemann, D. Hydrogen Production by Heterogeneous Photocatalysis. In *Encyclopedia of Interfacial Chemistry*; Wandelt, K., Ed.; Elsevier: Oxford, UK, 2018; pp. 413–419. [CrossRef]
4. Kennedy, J.; Bahruji, H.; Bowker, M.; Davies, P.R.; Bouleghlimat, E.; Issarapanacheewin, S. Hydrogen generation by photocatalytic reforming of potential biofuels: Polyols, cyclic alcohols, and saccharides. *J. Photochem. Photobiol. A Chem.* **2018**, *356*, 451–456. [CrossRef]
5. AlSalka, Y. Photocatalytic Water Splitting for Solar Hydrogen Production and Simultaneous Decontamination of Organic Pollutants. Ph.D. Thesis, Gottfried Wilhelm Leibniz Universität, Hannover, Germany, 8 July 2020.
6. Schneider, J.; Matsuoka, M.; Takeuchi, M.; Zhang, J.; Horiuchi, Y.; Anpo, M.; Bahnemann, D.W. Understanding TiO_2 Photocatalysis: Mechanisms and Materials. *Chem. Rev.* **2014**, *114*, 9919–9986. [CrossRef]
7. Pellegrin, Y.; Odobel, F. Sacrificial electron donor reagents for solar fuel production. *C. R. Chim.* **2017**, *20*, 283–295. [CrossRef]
8. Al-Madanat, O.; AlSalka, Y.; Ramadan, W.; Bahnemann, D.W. TiO_2 Photocatalysis for the Transformation of Aromatic Water Pollutants into Fuels. *Catalysts* **2021**, *11*, 317. [CrossRef]
9. Puga, A.V. Photocatalytic production of hydrogen from biomass-derived feedstocks. *Coord. Chem. Rev.* **2016**, *315*, 1–66. [CrossRef]
10. Ramadan, W.; Dillert, R.; Koch, J.; Tegenkamp, C.; Bahnemann, D.W. Changes in the solid-state properties of bismuth iron oxide during the photocatalytic reformation of formic acid. *Catal. Today* **2019**, *326*, 22–29. [CrossRef]
11. Friehs, E.; AlSalka, Y.; Jonczyk, R.; Lavrentieva, A.; Jochums, A.; Walter, J.-G.; Stahl, F.; Scheper, T.; Bahnemann, D. Toxicity, phototoxicity and biocidal activity of nanoparticles employed in photocatalysis. *J. Photochem. Photobiol. C Photochem. Rev.* **2016**, *29*, 1–28. [CrossRef]
12. AlSalka, Y.; Hakki, A.; Schneider, J.; Bahnemann, D.W. Co-catalyst-free photocatalytic hydrogen evolution on TiO_2: Synthesis of optimized photocatalyst through statistical material science. *Appl. Catal. B Environ.* **2018**, *238*, 422–433. [CrossRef]
13. Ramadan, W.; Feldhoff, A.; Bahnemann, D. Assessing the photocatalytic oxygen evolution reaction of $BiFeO_3$ loaded with IrO_2 nanoparticles as cocatalyst. *Sol. Energy Mater. Sol. Cells* **2021**, *232*, 111349. [CrossRef]
14. AlSalka, Y.; Granone, L.I.; Ramadan, W.; Hakki, A.; Dillert, R.; Bahnemann, D.W. Iron-based photocatalytic and photoelectrocatalytic nano-structures: Facts, perspectives, and expectations. *Appl. Catal. B Environ.* **2019**, *244*, 1065–1095. [CrossRef]
15. AlSalka, Y.; Al-Madanat, O.; Curti, M.; Hakki, A.; Bahnemann, D.W. Photocatalytic H_2 Evolution from Oxalic Acid: Effect of Cocatalysts and Carbon Dioxide Radical Anion on the Surface Charge Transfer Mechanisms. *ACS Appl. Energy Mater.* **2020**, *3*, 6678–6691. [CrossRef]
16. Li, Y.; Lu, G.; Li, S. Photocatalytic hydrogen generation and decomposition of oxalic acid over platinized TiO_2. *Appl. Catal. A Gen.* **2001**, *214*, 179–185. [CrossRef]
17. Franch, M.I.; Ayllón, J.A.; Peral, J.; Domènech, X. Photocatalytic degradation of short-chain organic diacids. *Catal. Today* **2002**, *76*, 221–233. [CrossRef]
18. Bowker, M.; Bahruji, H.; Kennedy, J.; Jones, W.; Hartley, G.; Morton, C. The Photocatalytic Window: Photo-Reforming of Organics and Water Splitting for Sustainable Hydrogen Production. *Catal. Lett.* **2015**, *145*, 214–219. [CrossRef]
19. Yamada, Y.; Miyahigashi, T.; Ohkubo, K.; Fukuzumi, S. Photocatalytic hydrogen evolution from carbon-neutral oxalate with 2-phenyl-4-(1-naphthyl)quinolinium ion and metal nanoparticles. *Phys. Chem. Chem. Phys.* **2012**, *14*, 10564–10571. [CrossRef]
20. AlSalka, Y.; Hakki, A.; Fleisch, M.; Bahnemann, D.W. Understanding the degradation pathways of oxalic acid in different photocatalytic systems: Towards simultaneous photocatalytic hydrogen evolution. *J. Photochem. Photobiol. A Chem.* **2018**, *366*, 81–90. [CrossRef]
21. Kmetykó, Á.; Mogyorósi, K.; Gerse, V.; Kónya, Z.; Pusztai, P.; Dombi, A.; Hernádi, K. Photocatalytic H_2 production using Pt-TiO_2 in the presence of oxalic acid: Influence of the noble metal size and the carrier gas flow rate. *Materials* **2014**, *7*, 7022–7038. [CrossRef]
22. Kandiel, T.A.; Ivanova, I.; Bahnemann, D.W. Long-term investigation of the photocatalytic hydrogen production on platinized TiO_2: An isotopic study. *Energy Environ. Sci.* **2014**, *7*, 1420–1425. [CrossRef]
23. Belhadj, H.; Hamid, S.; Robertson, P.K.J.; Bahnemann, D.W. Mechanisms of Simultaneous Hydrogen Production and Formaldehyde Oxidation in H_2O and D_2O over Platinized TiO_2. *ACS Catal.* **2017**, *7*, 4753–4758. [CrossRef]
24. Al-Madanat, O.; AlSalka, Y.; Curti, M.; Dillert, R.; Bahnemann, D.W. Mechanistic Insights into Hydrogen Evolution by Photocatalytic Reforming of Naphthalene. *ACS Catal.* **2020**, *10*, 7398–7412. [CrossRef]
25. Yuzawa, H.; Aoki, M.; Itoh, H.; Yoshida, H. Adsorption and Photoadsorption States of Benzene Derivatives on Titanium Oxide Studied by NMR. *J. Phys. Chem. Lett.* **2011**, *2*, 1868–1873. [CrossRef]
26. Yates, J.T., Jr.; McKee, D.W. Kinetic isotope effect in the heterogeneous reaction of graphite with H_2O (D_2O). *J. Chem. Phys.* **1981**, *75*, 2711–2714. [CrossRef]
27. Buettner, G.R. Spin Trapping: ESR parameters of spin adducts 1474 1528V. *Free Radic. Biol. Med.* **1987**, *3*, 259–303. [CrossRef]
28. Mendive, C.B.; Bredow, T.; Schneider, J.; Blesa, M.; Bahnemann, D. Oxalic acid at the TiO_2/water interface under UV (A) illumination: Surface reaction mechanisms. *J. Catal.* **2015**, *322*, 60–72. [CrossRef]

29. Draganic, Z.D.; Kosanic, M.; Nenadovic, M. Competition studies of the hydroxyl radical reactions in some gamma-ray irradiated aqueous solutions at different pH values. *J. Phys. Chem.* **1967**, *71*, 2390–2395. [CrossRef]
30. Doudrick, K.; Monzón, O.; Mangonon, A.; Hristovski, K.; Westerhoff, P. Nitrate reduction in water using commercial titanium dioxide photocatalysts (P25, P90, and Hombikat UV100). *J. Environ. Eng.* **2011**, *138*, 852–861. [CrossRef]
31. Mora-Sero, I.; Villarreal, T.L.; Bisquert, J.; Pitarch, Á.; Gomez, R.; Salvador, P. Photoelectrochemical behavior of nanostructured TiO_2 thin-film electrodes in contact with aqueous electrolytes containing dissolved pollutants: A model for distinguishing between direct and indirect interfacial hole transfer from photocurrent measurements. *J. Phys. Chem. B* **2005**, *109*, 3371–3380. [CrossRef]
32. Mulazzani, Q.G.; D'Angelantonio, M.; Venturi, M.; Hoffman, M.Z.; Rodgers, M.A. Interaction of formate and oxalate ions with radiation-generated radicals in aqueous solution. Methylviologen as a mechanistic probe. *J. Phys. Chem.* **1986**, *90*, 5347–5352. [CrossRef]
33. Yamada, Y.; Nomura, A.; Tadokoro, H.; Fukuzumi, S. A composite photocatalyst of an organic electron donor–acceptor dyad and a Pt catalyst supported on semiconductor nanosheets for efficient hydrogen evolution from oxalic acid. *Catal. Sci. Technol.* **2015**, *5*, 428–437. [CrossRef]
34. Sun, Y.; Chang, W.; Ji, H.; Chen, C.; Ma, W.; Zhao, J. An Unexpected Fluctuating Reactivity for Odd and Even Carbon Numbers in the TiO_2-Based Photocatalytic Decarboxylation of C_2-C_6 Dicarboxylic Acids. *Chem. A Eur. J.* **2014**, *20*, 1861–1870. [CrossRef] [PubMed]
35. Hykaway, N.; Sears, W.M.; Morisaki, H.; Morrison, S.R. Current-doubling reactions on titanium dioxide photoanodes. *J. Phys. Chem.* **1986**, *90*, 6663–6667. [CrossRef]
36. Nogami, G.; Kennedy, J.H. Investigation of "Current Doubling" Mechanism of Organic Compounds by the Rotating Ring Disk Electrode Technique. *J. Electrochem. Soc.* **1989**, *136*, 2583. [CrossRef]
37. Francàs, L.; Burns, E.; Steier, L.; Cha, H.; Solà-Hernández, L.; Li, X.; Shakya Tuladhar, P.; Bofill, R.; García-Antón, J.; Sala, X.; et al. Rational design of a neutral pH functional and stable organic photocathode. *Chem. Commun.* **2018**, *54*, 5732–5735. [CrossRef]
38. Puga, A.V.; Barka, N.; Imizcoz, M. Simultaneous H2 Production and Bleaching via Solar Photoreforming of Model Dye-polluted Wastewaters on Metal/Titania. *ChemCatChem* **2021**, *13*, 1513–1529. [CrossRef]
39. Bagotzky, V.S.; Osetrova, N.V. Investigations of hydrogen ionization on platinum with the help of micro-electrodes. *J. Electroanal. Chem. Interfacial Electrochem.* **1973**, *43*, 233–249. [CrossRef]
40. Gossenberger, F.; Roman, T.; Groß, A. Hydrogen and halide co-adsorption on Pt(111) in an electrochemical environment: A computational perspective. *Electrochim. Acta* **2016**, *216*, 152–159. [CrossRef]
41. Palominos, R.; Freer, J.; Mondaca, M.A.; Mansilla, H.D. Evidence for hole participation during the photocatalytic oxidation of the antibiotic flumequine. *J. Photochem. Photobiol. A Chem.* **2008**, *193*, 139–145. [CrossRef]
42. Schneider, J.T.; Firak, D.S.; Ribeiro, R.R.; Peralta-Zamora, P. Use of scavenger agents in heterogeneous photocatalysis: Truths, half-truths, and misinterpretations. *Phys. Chem. Chem. Phys.* **2020**, *22*, 15723–15733. [CrossRef]
43. Rowley, J.; Meyer, G.J. Reduction of I_2/I^{3-} by Titanium Dioxide. *J. Phys. Chem. C* **2009**, *113*, 18444–18447. [CrossRef]
44. Neta, P.; Huie, R.E.; Ross, A.B. Rate Constants for Reactions of Inorganic Radicals in Aqueous Solution. *J. Phys. Chem. Ref. Data* **1988**, *17*, 1027–1284. [CrossRef]
45. Ivanova, I.; Schneider, J.; Gutzmann, H.; Kliemann, J.-O.; Gärtner, F.; Klassen, T.; Bahnemann, D.; Mendive, C.B. Photocatalytic degradation of oxalic and dichloroacetic acid on TiO_2 coated metal substrates. *Catal. Today* **2013**, *209*, 84–90. [CrossRef]
46. Yamamoto, S.; Back, R.A. The gas-phase photochemistry of oxalic acid. *J. Phys. Chem.* **1985**, *89*, 622–625. [CrossRef]
47. Stoll, S.; Schweiger, A. EasySpin, a comprehensive software package for spectral simulation and analysis in EPR. *J. Magn. Reson.* **2006**, *178*, 42–55. [CrossRef] [PubMed]